Pergamon

Int. J. Heat Mass Transfer. Vol. 37, No. 17, pp. 2761–2769, 1994

0017–9310/94 $7.00+0.00

0017–9310(94)E0027–R

Mixed convection flow in curved annular ducts

HOON KI CHOI
Samsung Heavy Industries Research Institute, Munji-Dong, Yusung-Ku, Taejon, Korea

and

SEUNG O. PARK†
Department of Aerospace Engineering, Korea Advanced Institute of Science and Technology, Kusong-Dong, Yusung-Ku, Taejon, Korea

(*Received* 21 *October* 1993 *and in final form* 13 *January* 1994)

Abstract—Mixed convection flows in concentric curved annular ducts with constant wall temperature boundary condition are studied numerically. The flow is assumed to be fully developed so as to maintain a constant streamwise pressure and temperature gradient. Key parameters for the flow are the radius ratio (ratio of the inner core radius to the outer pipe radius), the Dean number, and the Grashof number. Computations are carried out for flows of various radius ratio with Dean numbers in the range 0–900 and Grashof numbers of 12.5 and 12 500. The secondary flow patterns, the streamwise velocity profiles and the heat transfer coefficients are presented. Effects of the Dean number and the Grashof number on the flow pattern, on the friction ratio (ratio of the friction for a curved annular duct to that for a straight annular duct flow), and on the heat transfer property are discussed based on the computational results. It is found that both the friction ratio and the Nusselt number ratio are strong functions of the radius ratio and the Dean number when $Gr = 12.5$, while these ratios do not change much with the radius ratio and the Dean number when $Gr = 12\,500$.

1. INTRODUCTION

A CONSIDERABLE amount of research effort has been directed toward the study of flow in curved pipes and thus numerous works have been published as can be found in the review article of Berger *et al.* [1]. Among these are the works concerning the mixed convection flow in curved pipes with heat transfer. Yao and Berger [2] investigated the fully developed laminar flow in a heated curved pipe by obtaining the power series solutions using regular pertubations in the Dean number and the product of the Reynolds and Rayleigh number. Prusa and Yao [3] presented numerical solutions of the mixed convection flow in a mildly coiled tube for various values of the Dean number and the product of the Reynolds number and the Rayleigh number. They obtained a flow-regime map which illustrates the centrifugal force dominant region, the buoyancy dominant region, and the region where both the centrifugal force and the buoyancy are important. Futagami and Aoyama [4] numerically and experimentally studied the laminar flow and heat transfer in a helically coiled tube for various combinations of the Dean number, the Prandtl number, and the product of the Reynolds and Rayleigh numbers. The secondary flow patterns and the average Nusselt number were presented.

Flows in curved annuli (i.e. tube-in-tube) with or without heat transfer, however, have received relatively scant attention. The flow in a curved annulus significantly differs from that in a curved circular tube owing to the presence of an inner wall boundary. Choi and Park [5] studied numerically the developing laminar flow in curved annuli. Evolution of secondary flow and the effect of radius ratio on the flow development were discussed in that work. Garimella *et al.* [6] investigated experimentally the forced convection heat transfer in coiled annular ducts in laminar and transitional flow regimes. Analytical solutions in power series form for mixed convection flow in mildly curved annular ducts with constant wall temperature condition were given by Karahalios [7]. In that work, however, the effect of the radius ratio on the flow was not properly treated. This deficiency was recently corrected by Park and Choi [8].

The interplay between the centrifugal force and the buoyancy in establishing the flow is an important aspect of the mixed convective flow in a curved annulus of a given radius ratio. The analytical approach, however, is rather limited to elucidate this complex interplay for a wider class of flows having various combinations of the Dean and the Grashof numbers. In this study, we thus attempt to investigate the mixed convective flow of curved annuli with various parameters by numerically solving a proper set of governing equations and to assess the effects of the centrifugal force and the buoyancy on the secondary flow and heat transfer.

† Author to whom correspondence should be addressed.

NOMENCLATURE

C_p	specific heat at constant pressure
Gr	Grashof number based on hydraulic radius, $g\beta\tau r_h^3/\nu^2$
g	gravitational acceleration
h	heat transfer coefficient
k	thermal conductivity
$\overline{Nu}$	overall average Nusselt number
Pr	Prandtl number
p	pressure
R	radius of curvature of the bend
Re	Reynolds number based on hydraulic radius, $r_h W_m/\nu$
r_i	inner radius of the annulus
r_o	outer radius of the annulus
r_h	hydraulic radius, $r_o - r_i$
T	temperature
T_o	reference temperature
t	time
v_r, v_ϕ, v_θ	r-, ϕ-, and θ-components of the non-dimensional velocity
r, ϕ, θ	toroidal coordinates.

Greek symbols

α	radius ratio, r_i/r_o
β	coefficient of thermal expansion
δ	curvature ratio based on the outer radius, r_o/R
δ_h	curvature ratio based on the hydraulic radius, r_h/R
Θ	non-dimensional temperature
κ	Dean number, $2Re\,\delta_h^{1/2}$
ρ	density
τ	temperature difference
ν	kinematic viscosity
Ψ	stream function for the secondary flow.

Subscript

c	curved annulus
m	mean value
s	straight annulus
w	wall surface.

Superscript

*	dimensional quantity.

We assume the flow to be fully developed both hydraulically and thermally as in previous works [2, 7, 8]. A pertinent characteristic length for the fully developed flow of the concentric annular duct is the hydraulic radius defined by $r_h = r_o - r_i$ [8]. Hence, the Reynolds number, the Dean number, and the Grashof number in this work are all based on r_h.

2. NUMERICAL DETAILS

A toroidal coordinate (r, ϕ, θ) system as shown in Fig. 1 was employed to formulate the problem. The fluid was assumed to have constant physical properties and to behave in accordance with the Boussinesq approximation. The flow was also assumed to be steady and laminar, and to have no internal heat generation. As mentioned earlier, we further assumed that the flow was fully developed under the constant streamwise pressure and temperature gradient conditions. The annular wall boundaries maintained a constant temperature at a given streamwise station. The dimensionless governing equations describing the conservation of mass, momentum and energy are respectively given as follows:

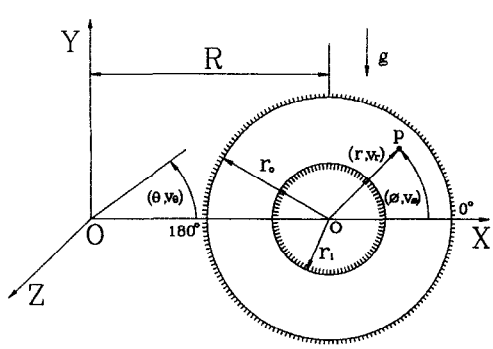

FIG. 1. Toroidal coordinate system for curved annulus.

$$\frac{1}{rB}\left[\frac{\partial}{\partial r}(rBv_r)+\frac{\partial}{\partial \phi}(Bv_\phi)\right]=0, \tag{1}$$

$$\frac{\partial v_r}{\partial t}+\frac{1}{rB}\left[\frac{\partial}{\partial r}(rBv_r^2)+\frac{\partial}{\partial \phi}(Bv_rv_\phi)\right]$$

$$-\frac{v_\phi^2}{r}-\frac{\delta v_\theta^2\cos\phi}{B}=-\frac{\partial p}{\partial r}+\frac{1}{Ro}\frac{1}{rB}\left[\frac{\partial}{\partial r}\left(rB\frac{\partial v_r}{\partial r}\right)\right.$$

$$\left.+\frac{\partial}{\partial \phi}\left(\frac{B}{r}\frac{\partial v_\phi}{\partial \phi}\right)\right]+\frac{Gr_o}{Ro^2}\Theta\sin\phi+S_r, \tag{2}$$

$$\frac{\partial v_\phi}{\partial t}+\frac{1}{rB}\left[\frac{\partial}{\partial r}(rBv_rv_\phi)+\frac{\partial}{\partial \phi}(Bv_\phi^2)\right]$$

$$+\frac{v_rv_\phi}{r}+\frac{\delta v_\theta^2\sin\phi}{B}=-\frac{1}{r}\frac{\partial p}{\partial \phi}+\frac{1}{Ro}\frac{1}{rB}\left[\frac{\partial}{\partial r}\left(rB\frac{\partial v_\phi}{\partial r}\right)\right.$$

$$\left.+\frac{\partial}{\partial \phi}\left(\frac{B}{r}\frac{\partial v_\phi}{\partial \phi}\right)\right]+\frac{Gr_o}{Ro^2}\Theta\cos\phi+S_\phi, \tag{3}$$

$$\frac{\partial v_\theta}{\partial t}+\frac{1}{rB}\left[\frac{\partial}{\partial r}(rBv_r v_\theta)+\frac{\partial}{\partial \phi}(Bv_\phi v_\theta)\right]+\frac{\delta v_\theta}{B}(v_r\cos\phi-v_\phi\sin\phi)=-\frac{\delta}{B}\frac{\partial p}{\partial\theta}+\frac{1}{Ro}\frac{1}{rB}\left[\frac{\partial}{\partial r}\left(rB\frac{\partial v_\theta}{\partial r}\right)+\frac{\partial}{\partial\phi}\left(\frac{B}{r}\frac{\partial v_\theta}{\partial\phi}\right)\right]+S_\theta, \quad (4)$$

$$\frac{\partial\Theta}{\partial t}+\frac{1}{rB}\left[\frac{\partial}{\partial r}(rBv_r\Theta)+\frac{\partial}{\partial\phi}(Bv_\phi\Theta)\right]=-\frac{\delta v_\theta}{B}\frac{\partial\Theta}{\partial\theta}+\frac{1}{Ro\,Pr}\frac{1}{rB}\left[\frac{\partial}{\partial r}\left(rB\frac{\partial\Theta}{\partial r}\right)+\frac{\partial}{\partial\phi}\left(\frac{B}{r}\frac{\partial\Theta}{\partial\phi}\right)\right]+S_\Theta, \quad (5)$$

where:

$$S_r=-\frac{1}{Ro}\left\{-\left[\left(2\frac{\partial v_\phi}{\partial\phi}+v_r\right)\Big/r^2\right]+\delta v_\phi\sin\phi/rB-\delta^2\cos\phi(v_r\cos\phi-v_\phi\sin\phi)/B^2\right\}$$

$$S_\phi=-\frac{1}{Ro}\left\{-\left[\left(2\frac{\partial v_r}{\partial\phi}-v_\phi\right)\Big/r^2\right]-\delta v_r\sin\phi/rB-\delta^2\sin\phi(v_r\cos\phi-v_\phi\sin\phi)/B^2\right\}$$

$$S_\theta=\frac{1}{Ro}\frac{\delta^2 v_\theta}{B^2}$$

$$S_\Theta=-\frac{1}{Ro\,Pr}\frac{\delta}{rB}\frac{\partial}{\partial\theta}\left(\frac{r}{B}\frac{\partial\Theta}{\partial\theta}\right)$$

and

$$B=1+\delta r\cos\phi.$$

The variables in the equations above were non-dimensionalized as follows:

$$r^*=r_o r \quad \text{(length)}; \quad (6a)$$

$$v_r^*=W_o v_r,\quad v_\phi^*=W_o v_\phi,\quad v_\theta^*=W_o v_\theta \quad \text{(velocity)}; \quad (6b)$$

$$p^*=\rho W_o^2 p \quad \text{(pressure)}; \quad (6c)$$

$$T_w-T_o=\tau \quad \text{(temperature difference)};$$

$$T_w-T=\tau\Theta \quad \text{(temperature)}. \quad (6d)$$

The reference velocity W_o, the reference Reynolds number R_o, and the reference Grashof number Gr_o employed in equations (2)–(6) were defined as

$$W_o=\left[\frac{r_o}{\rho R}\left(-\frac{\partial p^*}{\partial\theta}\right)\right]^{1/2}, \quad (7)$$

$$R_o=\frac{W_o r_o}{\nu}, \quad (8)$$

$$Gr_o=\frac{g\beta\tau r_o^3}{\nu^2}. \quad (9)$$

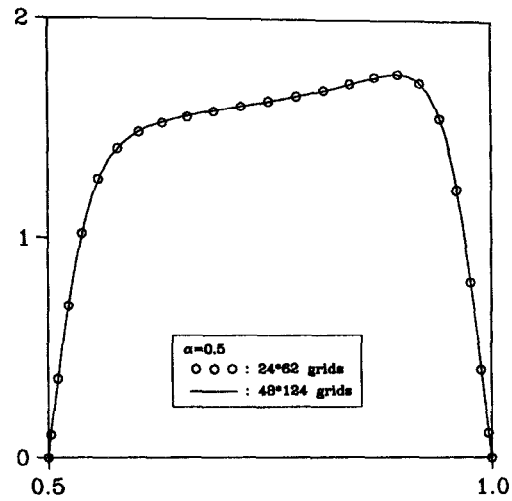

FIG. 2. Grid effects on the streamwise velocity profile along the line of symmetry ($\phi = 0°$) for $\alpha = 0.5$, $\kappa = 822$.

Equations (1)–(5) are subjected to the following boundary conditions:

$$v_r=v_\phi=v_\theta=\Theta=0 \quad \text{at } r=\alpha \text{ and } 1. \quad (10)$$

Local time derivative terms in the equations above were added mainly for computational convenience. For the numerical integration of equations (1)–(5) to obtain steady-state solutions, we adopted Chorin's [9] artificial compressibility method where an artificial compressibility term (an unsteady pseudo-pressure term) was added to equation (1). All the spatial derivatives were centrally differenced and the pseudo-time derivatives were discretized by the forward difference formula. The resulting algebraic system was solved by a factored ADI scheme as in Soh and Berger [10]. From 22 to 28 grid points along radial lines, depending on the radius ratio, were distributed unevenly to place more points in the viscous wall region, and 62 grid points were uniformly distributed in the circumferential direction. As a check for grid independency of solution, we performed the calculation on two different grid systems for the case of $\alpha = 0.5$. A typical result is contained in Fig. 2. We see that the 24×62 grid system yields a velocity profile as accurate as that with the 48×124 grid system.

3. RESULTS AND DISCUSSION

The flow characteristics dictated by the secondary motion are expected to differ by the relative importance of the centrifugal and the buoyancy forces. To examine the property of detailed flow features, computations were carried out for the flows with the Dean number varying in the range $0 < \kappa < 900$, and the radius ratio in the range 0.1–0.8. The Grashof number was set to be either 12.5 or 12 500. The Prandtl number was taken to be unity for all the cases.

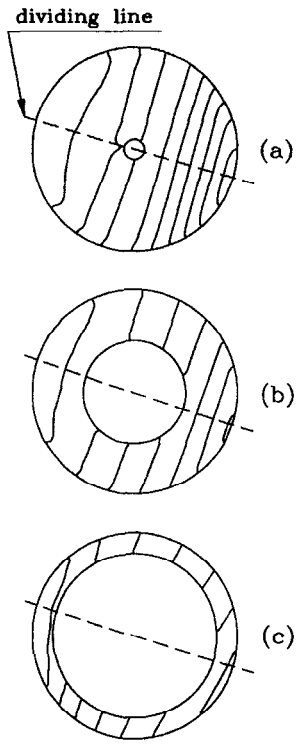

FIG. 3. Plots of the iso-pressure distributions for $\kappa = 822$ and $Gr = 12\,500$: (a) $\alpha = 0.1$; (b) $\alpha = 0.5$; and (c) $\alpha = 0.8$.

Pressure distribution

When the buoyancy is absent in a curved annular flow, we expect the iso-pressure lines to be nearly vertical (normal to the line of symmetry which is horizontal in our coordinate system of Fig. 1) since the pressure gradient balances the centrifugal force. On the other hand, when only the buoyancy force is present (that is, we consider the case of a straight annular flow), the iso-pressure lines would be horizontal (vertical to the direction of gravity) since the pressure gradient is required to balance the buoyancy force. When both the centrifugal and the buoyancy forces take part in establishing the secondary flow, the iso-pressure lines would be inclined to the line of symmetry as depicted in Fig. 3. Figure 3a, b and c illustrates the iso-pressure lines for the cases of $\alpha = 0.1$, 0.5, and 0.8, respectively. The Dean number, κ, is 822 and the Grashof number, Gr, is 12 500 for all these cases, both numbers being based on the hydraulic radius. We clearly see that the inclination angles of the iso-pressure lines shown are about the same. This suggest that the inclination angles of the iso-pressure line are essentially determined by the ratio of the (effective) Dean number to the Grashof number. We are, however, reminded that the streamwise pressure gradient is dominantly governed by the radius ratio [8]. The dashed lines in Fig. 3 denote the dividing line which separates approximately the near-symmetric vortical cells in the cross-sectional streamline contour (see Figs. 4–6). A dividing line is approximately normal to the iso-pressure lines and passes through the center of the annular cross-section.

Secondary flow pattern

The stream function for the secondary flow ψ is defined by

$$v_r = \frac{1}{rB}\frac{\partial}{\partial\phi}(B\psi), \quad v_\phi = -\frac{1}{B}\frac{\partial}{\partial r}(B\psi). \tag{11}$$

Figure 4 illustrates the secondary flow pattern for the case of $\alpha = 0.1$. When the Grashof number is 12.5, the flow motion is seen to be dominated by the centrifugal force as depicted in Fig. 4a-i and b-i. The secondary flow consists of two pairs of counter-rotating vortices placed symmetrically with respect to the plane of symmetry. The fluid particles near the inner and outer wall region move inward (i.e. toward the center of the curvature) owing to the pressure gradient set up by the centrifugal action of the outward moving particles in the core region. The secondary flow patterns of Fig. 4a-i and b-i characterized by the two symmetric vortices below and above the horizontal line are very similar to those observed in Choi and Park's work [9] for the developing flow with zero Grashof number. We further note that the center of the vortices moves toward the inside bend as the Dean number increases. When the Grashof number is 12 500, the vortical cells become inclined as seen in Fig. 4a-ii and b-ii; the degree of inclination changes with the ratio of the Dean number to the Grashof number. For the case of small Dean number and large Grashof number, the vortical cells line up almost vertically as shown in Fig. 4a-ii. An interesting feature of the secondary flow for the case with significant buoyancy effect (Fig. 4a and b-ii) is that the secondary flow streamlines become more complicated when compared to those with negligible buoyancy effect (Fig. 4a

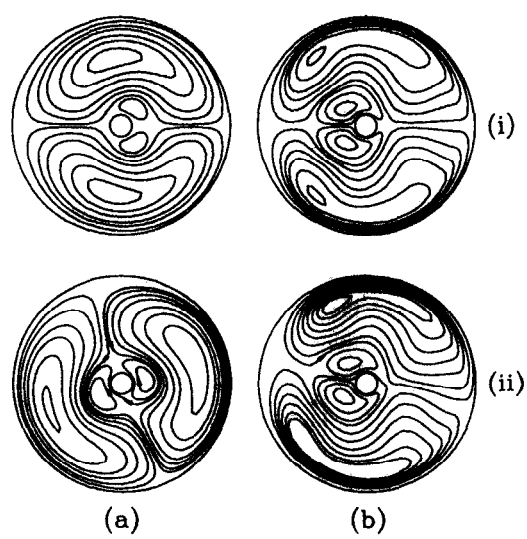

FIG. 4. Isostream streamline contours for $\alpha = 0.1$: (a) $\kappa = 95$; (b) $\kappa = 822$; (i) $Gr = 12.5$; and (ii) $Gr = 12\,500$.

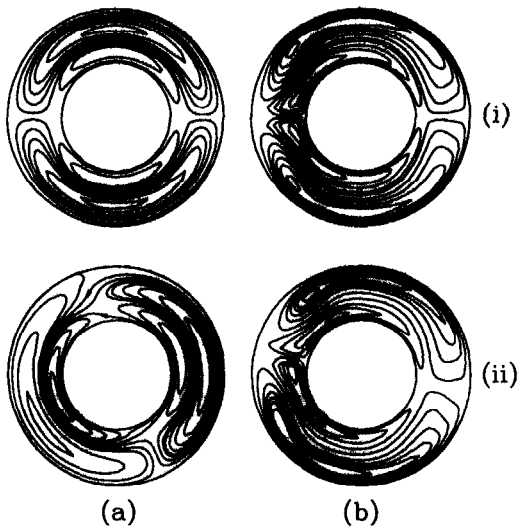

FIG. 5. Isostream streamline contours for $\alpha = 0.5$: (a) $\kappa = 95$; (b) $\kappa = 822$; (i) $Gr = 12.5$; and (ii) $Gr = 12\,500$.

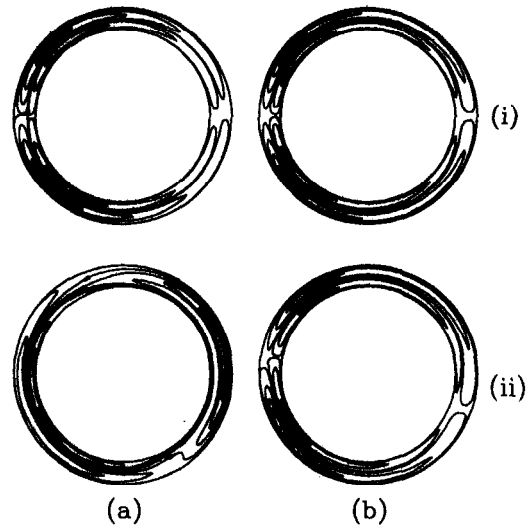

FIG. 6. Isostream streamline contours for $\alpha = 0.8$: (a) $\kappa = 95$; (b) $\kappa = 822$; (i) $Gr = 12.5$; and (ii) $Gr = 12\,500$.

and b-i). Note that a streamline encircles the inner cylinder in Fig. 4a-ii and b-ii. The vortical cells are asymmetric. This asymmetric property of the vortical cells for the case of curved pipe flow when the Grashof number is large has been demonstrated by Futagami and Aoyama [4]. We comment here that the concept of a dividing line which separates a pair of vortical cells confined in a half plane becomes ambiguous because of this asymmetry if the buoyancy effect is significant. In an approximate sense, however, the dividing line (if we define roughly the dividing line to distinguish the half plane containing the two centers of the vortical cells) turns away from the $\phi = 0°$–$180°$ (horizontal) line toward the $\phi = 90°$–$270°$ (vertical) line as the Grashof number increases for a given Dean number.

Figure 5 shows secondary flow streamlines when $\alpha = 0.5$. The (effective) Dean and Grashof numbers are the same as those of the corresponding cases of Fig. 4. Characteristic features such as the number of vortical cells, the inclination of the dividing line, and the symmetry property seen in Fig. 5 remain unchanged from those of Fig. 4. However, the strength of the inner cell vortices is seen to increase considerably owing to the larger radius of the inner pipe for these cases.

As an extreme case, the secondary flow when $\alpha = 0.8$ is illustrated in Fig. 6. In contrast to the two cases discussed above, the viscous effect is anticipated to be much greater because of the narrow gap between the inner and outer walls. Topological features of the flow, however, remain unaltered for this case also. The strengths of the inner and outer vortices are about the same.

Streamwise velocity

Owing to the secondary motion, the streamwise velocity profile for a curved annulus becomes considerably different from that of a straight annulus. For example, the position of the maximum streamwise velocity shifts toward the outside bend for a curved annular flow. A convenient measure to quantify the shift of the streamwise velocity is the first moment of the streamwise velocity about the center of the annulus [11]. The first moment in the x-direction is given by

$$Mo_x = \frac{\int_0^{2\pi}\int_{r_i}^{r_o} \frac{v_\theta x}{r_o} r\,dr\,d\phi}{\int_0^{2\pi}\int_{r_i}^{r_o} v_\theta r\,dr\,d\phi}. \tag{12}$$

The shift of the streamwise velocity in the y-direction Mo_y is similarly defined. If the streamwise velocity profile is uniform or symmetric about the center of the annulus, Mo_x and Mo_y will be zero. Mo_x would be positive if the average streamwise velocity over the the outside half plane is greater than that over the inside half plane; Mo_y would be positive if the average streamwise velocity over the upper half plane is greater than that over the lower half plane.

Figure 7 shows the change of Mo_x and Mo_y, when $\alpha = 0.1$, with the Dean number for the two given Grashof numbers. If the Dean number is very small so that the square root of it becomes smaller than about 5, Mo_x is seen to be negative, indicating that the streamwise flow shifts toward the inside bend. For this case of a very small Dean number, the flow passage is very loosely curved so that the viscous force rather than the centrifugal force is expected to be most influential in shaping the streamwise flow. Since the wall boundary along the streamwise direction of the outside half plane is longer than that of the inside half plane, the streamwise flow of the outside half plane experiences more friction than the flow of the inside half. The shift of Mo_x for the region of small Dean

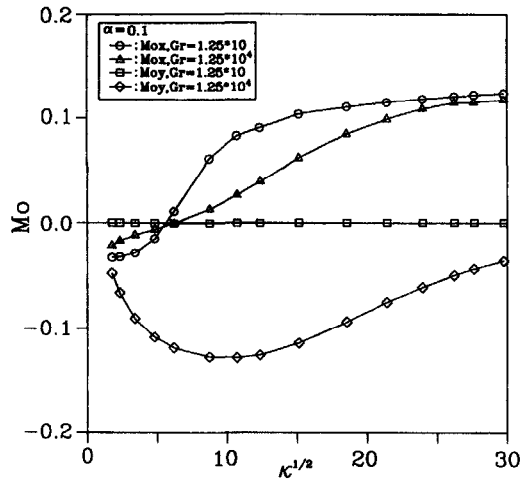

FIG. 7. Variation of first moment of streamwise velocity for $\alpha = 0.1$.

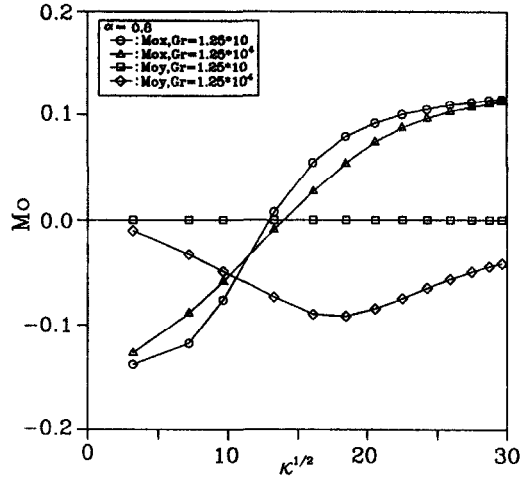

FIG. 9. Variation of first moment of streamwise velocity for $\alpha = 0.8$.

number becomes severer if the radius ratio becomes larger owing to the increased role of viscous forces as seen in Figs. 8 and 9. The appearance of a negative value of Mo_x in the developing flow of a loosely curved annulus was also discussed in our earlier work [5]. The variations of Mo_x and Mo_y with the Dean number for the cases of $\alpha = 0.5$ and 0.8 are shown in Figs. 8 and 9, respectively. As the Dean number increases, the streamwise flow shifts to the outside bend so that Mo_x becomes positive. The increase of Mo_x with the Dean number is rapid around the cross-over point from the negative to the positive value. For the region of large Dean number, the increase of Mo_x is somewhat gradual. Comparing the Mo_x curves for the two Grashof numbers, we find that the buoyancy force tends to slow down the outward shift of the streamwise flow; the increase of Mo_x with κ is milder when the Grashof number is larger.

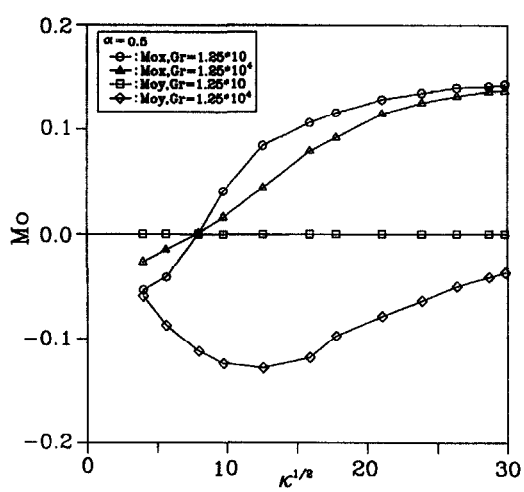

FIG. 8. Variation of first moment of streamwise velocity for $\alpha = 0.5$.

The effect of the Grashof number on the shift of streamwise velocity is better illustrated by the variation of Mo_y. The buoyancy force induces downward secondary motion in the core region as the secondary flow patterns illustrate, and hence renders Mo_y negative. Figures 7–9 show that Mo_y is zero when $Gr = 12.5$ while it is negative when $Gr = 12\,500$. Mo_y curves for the higher Gr indicate that the downward shift represented by the negative values of Mo_y first increases with κ for the small Dean number region and then decreases with κ for the higher Dean number region. This reveals an interesting fact that the increase of curvature for a loosely curved flow enhances the downward shift of the streamwise flow due to buoyancy while the increase of curvature for a non-loosely curved flow mitigates the downward shift.

We also notice, from Figs. 7–9, that the Dean number at which Mo_y becomes zero increases with the radius ratio; when the radius ratio increases, the viscous force increases accordingly and this deters the centrifugal force from taking effect so that the Dean number of the cross-over point of Mo_y increases. Similarly, the Dean number at which Mo_y becomes minimum (when $Gr = 12\,500$) gets larger as the radius ratio increases.

Temperature distributions

An isometric representation of the non-dimensional temperature, Θ, is shown in Fig. 10 for the case of $\alpha = 0.1$. When the buoyancy force is negligible ($Gr = 12.5$), the maximum temperature occurs at a point near the outside bend as depicted in Fig. 10a-i and b-i. For the case of $Gr = 12\,500$, the location of the maximum temperature moves towards the bottom wall as seen from Fig. 10a-ii and b-ii. The temperature gradient near the outside wall becomes steeper as the Dean number increases. The temperature distributions appear to be symmetric about the dividing line for all the cases shown.

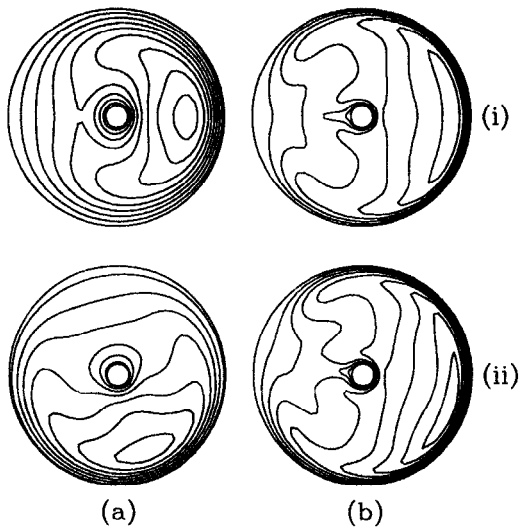

FIG. 10. Isothermal lines for $\alpha = 0.1$: (a) $\kappa = 95$; (b) $\kappa = 822$; (i) $Gr = 12.5$; and (ii) $Gr = 12\,500$.

Friction ratio

The secondary flow in a curved duct is generally known to result in a larger pressure drop in the streamwise direction when compared to that for a straight duct. Suppose that the flow rate for a curved annulus and that for a straight annulus are the same. The friction ratio f_c/f_s, the ratio of the streamwise pressure drop in the curved annulus to that in the straight annulus, is given by

$$\frac{f_c}{f_s} = \left(\frac{1}{R}\frac{\partial p^*}{\partial \theta}\right) \Big/ \left(\frac{\partial p^*}{\partial s^*}\right) \tag{13}$$

where s^* is the dimensional streamwise distance in the straight annular duct.

Variations of the friction ratio with $\kappa^{1/2}$ for some given values of α and Gr are plotted in Fig. 11. Except for the low Dean number region, the friction ratio is seen to vary linearly with $\kappa^{1/2}$. For curved pipe flows, this tendency has been observed by Barua [12], Mori and Nakayama [13, 14], and Soh and Berger [10].

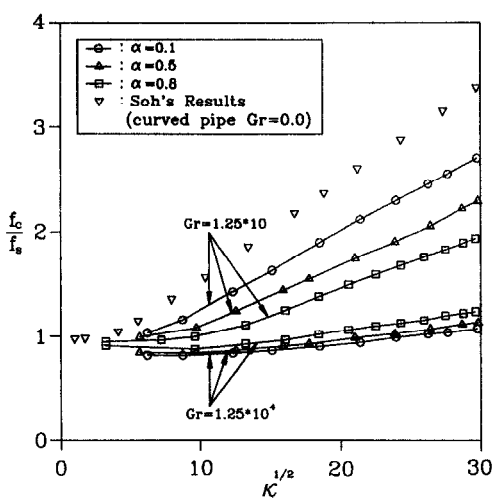

FIG. 11. Variation of the friction ratio.

When $Gr = 12.5$, the friction ratio becomes smaller as α increases for a given value of κ. The friction ratio is greatest for a curved pipe flow ($\alpha = 0$). When α becomes larger, the gap between the outer and inner wall becomes narrower, resulting in a strong viscous force. This weakens the effect of the centrifugal force and hence the secondary flow becomes less vigorous. We expect that $f_c/f_s \to 1$ for the limiting case $\alpha \to 1$. When $Gr = 12\,500$, the variation of the friction ratio with the radius ratio is quite contrary to the case of $Gr = 12.5$; the friction ratio for a given κ decreases as α increases. We also find that the friction ratio for the case of $Gr = 12\,500$ is much smaller than that for the case of $Gr = 12.5$. Further, the friction ratio is smaller than unity for a wider range of κ, suggesting that the secondary flow due to buoyancy in a straight annulus is more vigorous than that in a curved annulus when κ is not very large. The friction ratio for the case of $\alpha = 0.8$ and $Gr = 12.5$ is slightly smaller than unity when κ is very small. We consider that this is essentially the same phenomenon as the less-than-unity friction ratio for the case of $Gr = 12\,500$. When κ is very small, the buoyancy effect is greater for the secondary flow than for the curvature effect and this secondary motion is somewhat stronger for a straight annulus than for a curved annulus, resulting in a less-than-unity friction ratio. Comparing the curves for $Gr = 12.5$ and $12\,500$, we find that the effect of radius ratio on the friction ratio is much smaller when $Gr = 12\,500$.

Heat transfer rate

A common finding is that the secondary flow enhances heat transfer rates. To examine the heat transfer property for the present work, we first consider the energy balance of an infinitesimal element of length $R\,\mathrm{d}\theta$. We have

$$\rho C_p \bar{v}_\theta^* \pi (r_o^2 - r_i^2)\,\mathrm{d}T = 2\pi(r_o + r_i) R\,\mathrm{d}\theta \bar{h}(T_m - T_w), \tag{14}$$

where T_m is the local bulk temperature and T_w is the wall temperature. The perimeter average heat transfer coefficient $\bar{h}$ is expressed by

$$\bar{h} = \frac{h_o' + \alpha h_i'}{1 + \alpha}, \tag{15}$$

where h_i' and h_o' are the average heat transfer coefficient at the inner and the outer walls, respectively. Using equation (14), the overall average Nusselt number taken for the annulus is given by

$$\begin{aligned} \overline{Nu}_c &= \frac{2\bar{h} r_h}{k} \\ &= \frac{(r_o^2 - r_i^2)}{r_o + r_i} \frac{\rho C_p r_h}{k} \bar{v}_0 \frac{1}{R} \frac{\mathrm{d}\Theta}{\mathrm{d}\theta} \frac{W_o}{\Theta_m} \\ &= (1-\alpha)^2 \delta\, Pr\, Ro_c \frac{\bar{v}_\theta}{\Theta_m} \frac{\mathrm{d}\Theta}{\mathrm{d}\theta}, \end{aligned} \tag{16}$$

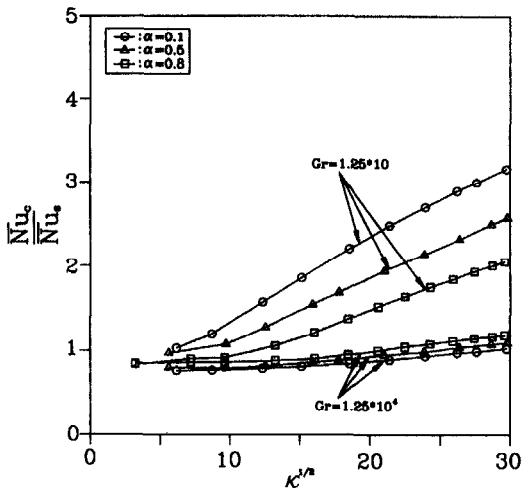

FIG. 12. Variation of the overall average Nusselt number ratio.

where Ro_c is the Reynolds number based on the outer pipe radius and the subscript c denotes the curved annulus. The non-dimensional bulk temperature Θ_m is defined by

$$\Theta_m = \frac{\int_0^{2\pi}\int_{r_i}^{r_o} \Theta v_\theta r \, dr \, d\phi}{\int_0^{2\pi}\int_{r_i}^{r_o} v_\theta r \, dr \, d\phi}. \quad (17)$$

The overall average Nusselt number for a straight annulus is similarly given by

$$\overline{Nu}_s = (1-\alpha)^2 \, Pr \, Ro_s \frac{\bar{v}_s}{\Theta_m} \frac{d\Theta}{ds}. \quad (18)$$

The Nusselt number ratio $\overline{Nu}_c/\overline{Nu}_s$ is obtained from equations (16) and (18). Figure 12 contains the curves of this ratio which clearly demonstrate that the Nusselt number ratio behaves in the same manner as the friction ratio. We see that $\overline{Nu}_c/\overline{Nu}_s$ is proportional to $\kappa^{1/2}$ when the Dean number is not very small, as has been observed in the case of the friction ratio. The dependency of the Nusselt number ratio on the Dean number and on the radius ratio is much greater when $Gr = 12.5$; when $Gr = 12\,500$, the ratio does not change much with either the Dean number or the radius ratio. As was the case for the friction ratio, when $Gr = 12\,500$, the Nusselt number for curved annular flow is not largely different from that for straight annular flow so that the ratio of the two is about unity. Similar observations for curved pipe flows have been made by Mori and Nakayama [13, 14] and Prusa and Yao [3]. When $Gr = 12.5$, the Nusselt number ratio decreases with the increase of the radius ratio for a given Dean number and increases with the Dean number for a given radius ratio. On the contrary, when $Gr = 12\,500$, the Nusselt number ratio increases as the radius ratio increases. Further, the ratio is a little smaller than 1 over a wide range of the Dean number, indicating that the overall average Nusselt number for a straight annulus is somewhat greater than that for a curved annulus.

4. CONCLUSIONS

Fully developed mixed convection flow in curved annular ducts with a constant wall temperature boundary was investigated numerically. The following was found.

The secondary flow pattern is nearly symmetric about the (horizontal) dividing line when the centrifugal force effect is large compared to the buoyancy force effect. As the Grashof number increases, the dividing line rotates away from the horizontal position. If the Grashof number increases further, the secondary flow pattern exhibits strong asymmetry. When the Dean number is very small, Mo_x is negative, indicating that more mass is flowing through the inside half of the annulus. As the Dean number increases, Mo_x becomes positive, reflecting the outward shift of the flow due to the centrifugal force effect. When $Gr = 12\,500$, Mo_y is negative. For a given radius ratio, Mo_y decreases with the Dean number up to a certain point at which Mo_y becomes minimum and then increases with the Dean number.

When $Gr = 12.5$ (negligible buoyancy), the friction ratio and the Nusselt number ratio decrease as the radius ratio increases for a given Dean number. For a given radius ratio, these friction and heat transfer ratios are much greater than 1, signifying that the curved annular duct flow has more friction and heat transfer than the straight annular duct flow. It was found that the friction ratio and the Nusselt number ratio proportionally increase with $\kappa^{1/2}$ when κ is not very small. When $Gr = 12\,500$, the friction and the Nusselt number ratios do not change much with either the Dean number or the radius ratio. Interestingly, these ratios increase as the radius ratio increases, contrary to the case of $Gr = 12.5$. When κ is not large (say, smaller than 600), the friction and the Nusselt number ratio are less than 1, signifying that the secondary flow in a straight annular duct is stronger than that in a curved annular duct, again contrary to the case of $Gr = 12.5$.

REFERENCES

1. S. A. Berger, L. Talbot and L. S. Yao, *Ann. Rev. Fluid Mech.* **15**, 461–512 (1983).
2. L. S. Yao and S. A. Berger, *J. Fluid Mech.* **88**, 339–354 (1978).
3. J. Prusa and L. S. Yao, *J. Fluid Mech.* **123**, 503–522 (1982).
4. K. Futagami and Y. Aoyama, *Int. J. Heat Mass Transfer* **31**, 387–396 (1988).
5. H. K. Choi and S. O. Park, *Int. J. Heat Fluid Flow* **13**, 41–49 (1992).
6. S. Garimella, D. E. Richards and R. N. Christensen, *J. Heat Transfer* **110**, 329–336 (1988).
7. G. T. Karahalios, *Phys. Fluids A* **2**, 2164–2175 (1990).

8. S. O. Park and H. K. Choi, *Phys. Fluids A* **5,** 1843–1845 (1993).
9. A. J. Chorin, *J. Comp. Phys.* **2,** 12 (1967).
10. W. Y. Soh and S. A. Berger, *Int. J. Numer. Methods Fluids* **7,** 733–755 (1987).
11. D. E. Olson and B. Snyder, *J. Fluid Mech.* **150,** 139–158 (1985).
12. S. N. Barua, *Q. J. Mech. Appl. Math.* **16,** 61–77 (1963).
13. Y. Mori and W. Nakayama, *Int. J. Heat Mass Transfer* **8,** 67–82 (1965).
14. Y. Mori and W. Nakayama, *Int. J. Heat Mass Transfer* **10,** 681–695 (1967).